Journal of Power Sources 196 (2011) 6325–6331

Contents lists available at ScienceDirect

Journal of Power Sources

journal homepage: www.elsevier.com/locate/jpowsour

Microstructure, property and processing relation in gradient porous cathode of solid oxide fuel cells using statistical continuum mechanics

Hoda Amani Hamedani [a,*], Majid Baniassadi [b,c], M. Khaleel [d], Xin Sun [d], S. Ahzi [b], D.Ruch [c], H. Garmestani [a]

[a] School of Materials Science and Engineering, Georgia Institute of Technology, 771 Ferst Dr., N.W., Atlanta, GA 30332-0245, USA
[b] University of Strasbourg, IMFS, 2 Rue Boussingault, 67000 Strasbourg, France
[c] Centre de Recherche Public Henri Tudor, AMS, 70 Rue de Luxembourg, L-4221 Esch-sur-Alzette, Luxembourg
[d] Fundamental and Computational Sciences Directorate, Pacific Northwest National Laboratory, Richland, WA 99354, United States

ARTICLE INFO

Article history:
Received 22 January 2011
Received in revised form 19 March 2011
Accepted 23 March 2011
Available online 1 April 2011

Keywords:
Solid oxide fuel cells
Functionally graded materials (FGM)
Porous cathode
Probability functions
Electrical conductivity

ABSTRACT

This paper investigates the relation between microstructure, macroscopic transport properties, and fabrication processing for a gradient porous cathode of solid oxide fuel cells (SOFCs). Functionally graded porous cathode with smooth variations in pore size is composed of lanthanum strontium manganite (LSM) fabricated on yttria stabilized zirconia (YSZ) electrolyte substrate using a multi-step spray pyrolysis (SP) technique at various deposition conditions. Two-dimensional (2D) serial-sections of the gradient porous microstructure obtained by FIB–SEM are fully characterized using statistical correlation functions. Results of statistical analysis of the microstructures revealed that the SP processing technique is capable of generating statistically identical and homogeneous microstructures with smooth gradient in pore size resulting from changing the processing parameters. Strong contrast statistical approach is also used to predict the in-plane temperature dependent effective electrical conductivity of the gradient porous cathode and the results are compared to the experimental data.

1. Introduction

SOFCs are highly efficient, environmentally friendly, and fuel-flexible electrochemical devices as an alternative power source for next-generation energy systems. Extensive research is underway to meet the goals toward commercialization of these devices. One major goal is to improve the performance and reliability of the cells while minimizing costs that are essentially associated with high operating temperatures (~800 to 1000 °C) and processing of SOFCs. Previous studies have shown some progress toward this goal mainly aimed at design of functionalized materials/microstructures that operate efficiently at lower temperatures (<800 °C) [1–4]. A common way to improve the functionality of individual layers at low temperature is to apply functionally graded materials (FGMs) approach with compositional/microstructural variations such as pore size in some spatial direction [5–9]. In composition grading, volumetric ratios of the electronic conductor phase is mixed with ionic conductor electrolyte to form the composite electrode. Furthermore, particle/pore grading is implemented by having large particles/pores at the outer layers close to the surface for gas flow and gradually smaller pores at the interface with the electrolyte for diffusion and chemical reaction processes. In either ways, the goal is to enhance the electrochemical reactivity and increase the electronic/ionic conductivity of the electrode, to minimize the mass transport resistance to gas mixtures and thus concentration polarization inside the porous electrode and to increase mechanical stabilities.

Processing of the SOFCs electrodes are typically carried out using conventional processing techniques such as consolidation and sintering of ceramic powder [10,11]. However, deposition routes take the advantage of governing the processing parameters; thus, one can utilize these techniques over the conventional methods to optimize the microstructure of the SOFC components by making desirable variations in the microstructure [12,13]. Researchers have attempted to identify those processes that have a significant impact on cell performance [1]. Here, the role of microstructure is very critical as it acts as a direct link between processing, properties and performance of the fuel cell. However, all current manufacturing processes are stochastic in nature [1]; thus, an effective and meaningful understanding of the processing-microstructure-property relationships demands establishment of a framework (consisting of development of manufacturing processes with controllable processing parameters) that can account for these variations in constitutive laws [14].

* Corresponding author. Tel.: +140 4510 6386; fax: +167 8306 0630.
E-mail address: hamani3@gatech.edu (H.A. Hamedani).

0378-7753/$ – see front matter © 2011 Elsevier B.V. All rights reserved.
doi:10.1016/j.jpowsour.2011.03.046

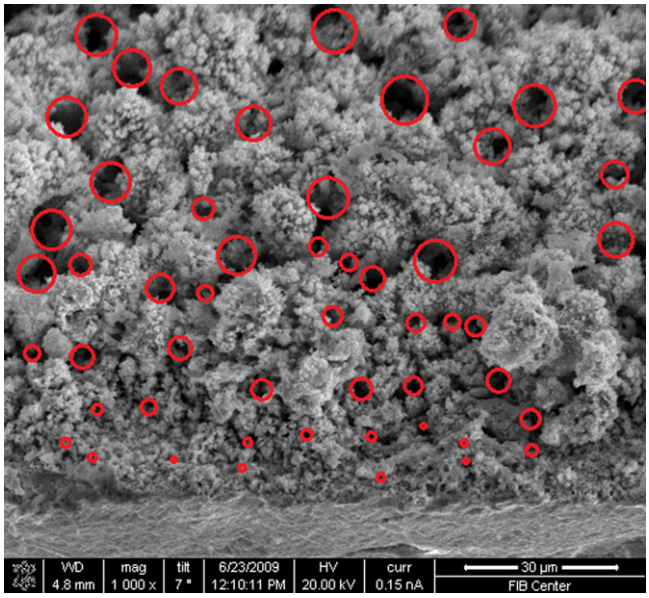

Fig. 1. SEM cross-section image of the functionally gradient porous LSM cathode deposited on top of YSZ electrolyte. Red circles show presence of large pores on the top layer and gradually smaller pores next to the electrode/electrolyte interface. (For interpretation of the references to color in this figure legend, the reader is referred to the web version of this paper.)

To this end, statistical continuum approaches have been developed based on probability functions to account for more details of microstructure heterogeneities. One general approach for predicting the effective properties of a two-phase material with properties of each phase similar to the average is called "weak-contrast" expansion. However, in the case where the properties of the phases are highly dissimilar, "strong-contrast" theory is implemented. While most of the analyses reported in the literature are performed on finding the correlation between the microstructure and properties, correlation between the three microstructure, properties and processing parameters is less regarded. In this paper, statistical correlation functions are used to make a linkage between microstructure of a functionally graded LSM cathode to its properties and processing conditions. Gradient porous LSM cathodes are processed by a modified multi-step spray pyrolysis [15]. Variations in pore geometry, clustering behavior and percolation are also studied. Strong-contrast statistical continuum theory is also used to predict the effective conductivity of the porous LSM cathode through incorporation of the details of microstructure into correlation functions. Results are then compared to the experimental measurement data of the electrical conductivity.

2. Experimental

2.1. Sample preparation procedure

Continuously graded porous cathode functional layer was processed by a novel multi-step spray pyrolysis technique reported elsewhere [15]. The LSM was deposited on a 1 mm thick pellet of polycrystalline YSZ electrolyte by changing the deposition variables, such as solution flow rate, nozzle to substrate distance and temperature. The gradient in pore size is achieved by design of sequence of processing steps in SP including variation of deposition parameters in a controlled manner to create a fine microstructure containing small pores and nanocrystalline particles at the interface and gradually larger pores/particles at the outer layers close to the surface of the cathode as shown in Fig. 1. Variation in pore size in the gradient microstructure is highlighted by red circles of different sizes in the image; note that the SEM image is taken at 7° tilt angle for clear observation of the gradient in the pore size in the cathode layer.

2.2. Imaging technique

In porous brittle ceramic samples, due to low contrast at pore edges, electron microscopy is superior to optical microscopy methods that involve flat-polishing step for quantitative determination of pore dimensions [16,17]. In this work, the in-plane (x–y plane) microstructure of the processed gradient porous LSM cathode and its temperature dependent electrical conductivity in the corresponding direction is investigated. For this purpose, FEI Nanolab Nova200 dual-beam FIB/SEM was utilized to obtain microscopic two-dimensional (2D) SEM images in x–y plane by sectioning the gradient porous LSM specimen from the surface down to the electrolyte interface in vertical direction along z axis. Using Auto Slice and View software (FEI Co.) serial-sectioning of gradient porous LSM cathode was accomplished to observe variations in the microstructure in x, y, z directions. The dual-beam FIB/SEM is composed of ion beam which allows milling of the surface while the imaging is conducted by the electron gun. A number of LSM serial-section images were milled at highest current density (20 nA) and scanned at identical spacing of 100 nm along the thickness, i.e. the gradient (z) direction. Starting from the rough surface, a larger area of the gradient porous LSM sample was initially milled to obtain a flat surface for further accurate milling process. A set of seven 2D-SEM images (50 μm × 50 μm) at equal spacing of ~1.5 μm were chosen among serial-sections for characterization and as representative of the variations in pore size in the microstructure. These images were cut out of a larger (>50 μm × 50 μm) area to prevent inappropriate edge effects from the milling process. Then, using the threshold technique, images were converted from grayscale into binary (black-and-white); black pixels are associated to pore phase with a value of zero (phase 1) and white pixels having the value of one represent solid LSM phase (phase 2). Fig. 2 shows the schematic of milling process of gradient porous LSM cathode and seven binary images obtained for further microstructure analysis. As shown, the milling process is carried out starting from surface containing large pores and ending with smaller pores at the electrolyte interface.

Every two binary images correspond to a layer that has been processed at a specific deposition condition.

3. Microstructure characterization of gradient porous LSM cathode

3.1. n-Point correlation functions

Statistical homogenization techniques use n-point correlation functions to statistically describe distribution, orientation and geometry of the phases in the microstructure and to determine the effective physical properties of the heterogeneous media. In the case of porous media, one major morphological descriptor of the heterogeneous microstructure is the volume fraction of the phases (ϕ) or porosity that can be determined by calculating the one-point correlation function. In fact, one-point probability function represents only the volume fraction and gives no more information about the morphology (Eq. (1)). Thus, higher-order probability functions are exploited to access more details of the microstructure.

$$P_1^i(\boldsymbol{x}) = \phi_i \tag{1}$$

Two-point correlation function, $P_2^{ij}(x, x')$, is another probability function, if a vector $\vec{r}$ is thrown on a two-phase microstructure such

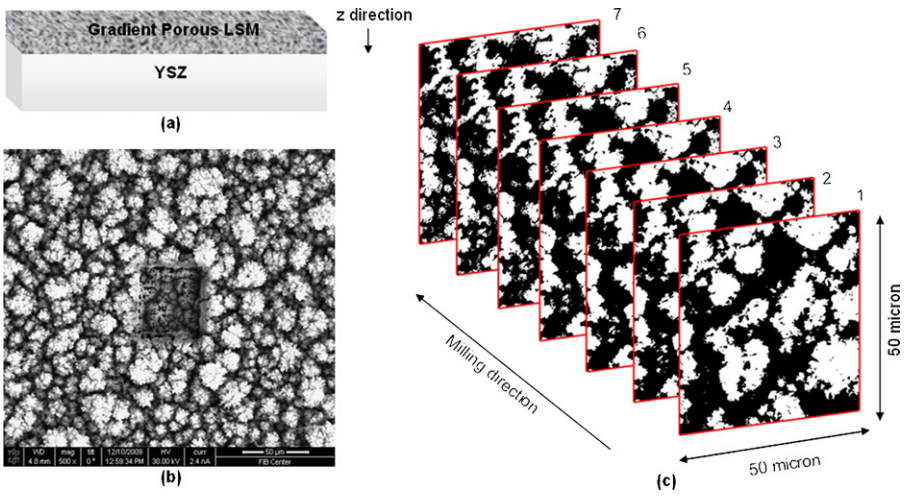

Fig. 2. (a) Schematic of gradient porous LSM cathode on YSZ electrolyte. (b) Top view of the milled area of the gradient porous LSM sample. (c) Set of binary serial-section images.

that the starting point of this vector lies at point x in phase i and its end lies at point x' in phase j:

$$P_2^{ij}(\boldsymbol{x}, \boldsymbol{x}') = P\left\{(\boldsymbol{x} \in i) \cap (\boldsymbol{x}' \in j)\right\} \quad i = 1, 2 \quad \text{and} \quad j = 1, 2 \tag{2}$$

The following relations hold for a two-phase microstructure:

$$P_2^{ii}(\boldsymbol{x}, \boldsymbol{x}') = \phi_i, \quad \text{and} \quad P_2^{ij}(\boldsymbol{x}, \boldsymbol{x}') = \phi_j \quad \left\|\vec{r}\right\| \to 0 \tag{3}$$

$$P_2^{ij}(\boldsymbol{x}, \boldsymbol{x}') = P_1^i(\boldsymbol{x}) \times P_1^j(\boldsymbol{x}') = \phi_i \phi_j \quad \left\|\vec{r}\right\| \to \infty \tag{4}$$

It turns out from (3) that:

$$P_2^{11} + P_2^{12} = \phi_1 \tag{5}$$

$$P_2^{21} + P_2^{22} = \phi_2 \tag{6}$$

$$P_2^{12} = P_2^{21} \tag{7}$$

$$P_2^{11} + P_2^{12} + P_2^{21} + P_2^{22} = 1 \tag{8}$$

thus, one of the above probabilities comes out as an independent variable. These correlation functions are generally analytically formulated by Corson in the form of an exponential regression function as in the following equation:

$$P_2^{ij}(\boldsymbol{r}) = \phi_i \phi_j + (-1)^{i+j} \phi_i \phi_j \exp(-c_{ij} \boldsymbol{r}^{n_{ij}}) \tag{9}$$

where c_{ij} and n_{ij} are empirical least square constants of the curve fitted to the experimental probability curves.

3.2. Pore-size distribution function

The main concern in characterization of the gradient porous microstructure is to realize the geometric variations of the pore phase (such as size, shape, etc.) along the gradient direction (z). In general, such geometrical information is not contained in the correlation functions. Based on a definition by Torquato, the pore-size distribution function $p^{(i)}(r)$ is defined by the probability of finding a pore with its length between r and $r + dr$ in phase (i) of interest. This information is useful for studying the transport properties and fluid flow in porous media [18]. Since the gradient porous microstructure is statistically isotropic in x and y directions, a test line of defined length can be thrown through the RVEs in either isotropic direction without changing the orientation. To this end, a MATLAB code was written to determine the length of the phase of interest (i.e., pores) in the direction of the test line. The program starts with scanning the RVEs in the horizontal (x) direction. The number of line scans is equal to the number of pixels in y direction for each image. The code counts the number of pixels in the given line segment for its binary value (denoted by 0 or 1) and gives the number of pixels contained completely in that particular phase. By normalizing the values, directional pore-size distribution functions for given RVE images of the gradient porous sample along z direction can be obtained.

3.3. Percolation and clustering functions

The study of clustering and percolation is important in prediction of transport properties in porous structures. It is performed by introducing a two-point correlation cluster function $C_2^{(i)}(x - x')$ which is the probability that both points x and x' are found in the same cluster of one of the phases to analyze the behavior of conduction and flow in porous microstructures. The information obtained from cluster function is not sufficiently contained in any of the lower-order microstructural functions described above [18]. Among different types of algorithms used for solving the percolation problem, an efficient percolation algorithm is used to check the continuity of cells for all clusters [19].

3.4. Strong contrast approximation of the effective conductivity

Strong-contrast approach in statistical continuum theory is used in this work to predict the effective electrical conductivity of the two-phase isotropic (porous) media based on the work of Torquato [20], where the individual properties of phases are highly dissimilar. Mikdam et al. have reported that strong-contrast formulation provides a better estimate for the effect of the microstructure on the conductivity for porous media [21,22]. The linear constitutive relationship can be generalized to describe the electrical and thermal conductivity.

The electrical conductivity σ at any arbitrary point x is related to the local current density $J(x)$ and the local electric field $E(x)$ by the Ohm's law:

$$\boldsymbol{J}(x) = \sigma_e(x) \cdot \boldsymbol{E}(x) \tag{10}$$

The local polarization field $P(x)$ is defined by

$$\boldsymbol{P}(x) = [\sigma_e(x) - \sigma_R]\boldsymbol{E}(x) \tag{11}$$

Since the current density is divergence free, we will have:

$$\nabla \cdot \boldsymbol{J}(x) = \sigma_R \nabla \cdot \boldsymbol{E}(x) + \nabla \cdot \boldsymbol{P}(x) = 0 \tag{12}$$

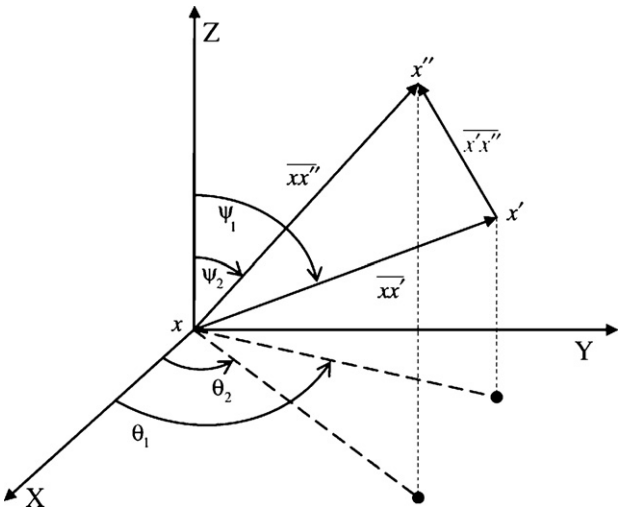

Fig. 3. Representation of vectors in spherical coordinate [25].

Here, a potential field $\varphi(x)$ is defined such that

$$\boldsymbol{E}(x) = \nabla\varphi \tag{13}$$

Thus, by substituting Eq. (13) in (12) we will obtain the following equation:

$$\nabla \cdot \boldsymbol{J}(x) = -\sigma_R \nabla \cdot (\phi(x)) + \nabla \cdot \boldsymbol{P}(x) = 0 \tag{14}$$

The solution to Eq. (14) can be obtained using Green's function and integration by parts. The reader is referred to [23] for details on derivation of the solution. Assuming isotropic properties of the phases, the effective conductivity tensor (σ_e) of the porous microstructure in any d-dimensional space can be obtained using the strong-contrast expansion as follows [21,24]:

$$\begin{aligned}
&\{\sigma_e - \sigma_R \boldsymbol{I}\}^{-1} . \{\sigma_e + (d-1)\sigma_R \boldsymbol{I}\} \\
&= \frac{1}{\beta_{SR} P_1^S(\boldsymbol{x})} \boldsymbol{I} - \sigma_R d \int \left[\frac{P_2^S(\boldsymbol{x}, \boldsymbol{x}') - P_1^S(\boldsymbol{x}) P_1^S(\boldsymbol{x}')}{P_1^S(\boldsymbol{x}) P_1^S(\boldsymbol{x}')} \right] H^R(\boldsymbol{x} - \boldsymbol{x}')\, dx' \\
&\quad - \sigma_R^2 d^2 \beta_{SR} \iint \left[\frac{P_3^S(\boldsymbol{x}, \boldsymbol{x}', \boldsymbol{x}'')}{P_1^S(\boldsymbol{x}) P_1^S(\boldsymbol{x}')} - \frac{P_2^S(\boldsymbol{x}, \boldsymbol{x}') P_2^S(\boldsymbol{x}', \boldsymbol{x}'')}{P_1^S(\boldsymbol{x}) P_1^S(\boldsymbol{x}') P_1^S(\boldsymbol{x}'')} \right] H^R(\boldsymbol{x} - \boldsymbol{x}') \\
&\quad \cdot H^R(\boldsymbol{x}' - \boldsymbol{x}'')\, d\boldsymbol{x}'\, d\boldsymbol{x}'' - \ldots
\end{aligned} \tag{15}$$

where I is the second-order identity tensor, β_{SR} is the polarizability, σ_R is the reference conductivity, and $\boldsymbol{H}^R(\boldsymbol{x} - \boldsymbol{x}')$ is a second-order tensor, defined below. The polarizability β_{SR} is expressed by:

$$\beta_{SR} = \frac{\sigma_S - \sigma_R}{\sigma_S + (d-1)\sigma_R} \tag{16}$$

The second-order tensor $\boldsymbol{H}^R(\boldsymbol{x} - \boldsymbol{x}')$ is defined by:

$$\boldsymbol{H}^R(\boldsymbol{x} - \boldsymbol{x}') = \frac{1}{\Omega\, \sigma_R} \frac{d\, nn - \boldsymbol{I}}{|\boldsymbol{x} - \boldsymbol{x}'|^d} \tag{17}$$

where Ω is the total solid angle contained in a d-dimensional sphere and

$$n = \frac{(\boldsymbol{x} - \boldsymbol{x}')}{|\boldsymbol{x} - \boldsymbol{x}'|} \tag{18}$$

Here, the three-point correlation function is estimated using the following approximation (with the representation of the corresponding vectors in spherical coordinates shown in Fig. 3) [25]:

$$P_3^s(\boldsymbol{x}, \boldsymbol{x}', \boldsymbol{x}'') \cong \left[\frac{|\boldsymbol{x}\boldsymbol{x}'|}{|\boldsymbol{x}\boldsymbol{x}'| + |\boldsymbol{x}\boldsymbol{x}''|} P_2^s(\boldsymbol{x}, \boldsymbol{x}'') + \frac{|\boldsymbol{x}\boldsymbol{x}''|}{|\boldsymbol{x}\boldsymbol{x}'| + |\boldsymbol{x}\boldsymbol{x}''|} P_2^s(\boldsymbol{x}, \boldsymbol{x}') \right] \frac{P_2^s(\boldsymbol{x}', \boldsymbol{x}'')}{P_1^s(\boldsymbol{x})} \tag{19}$$

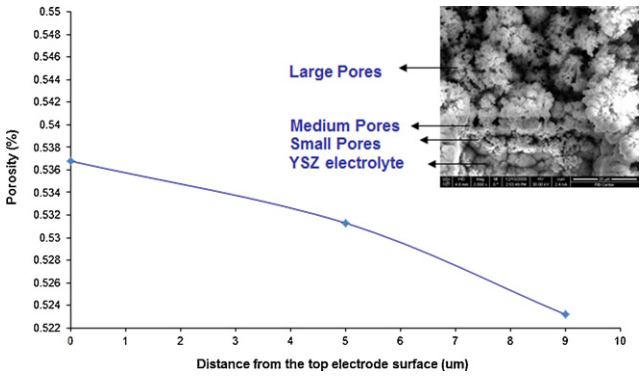

Fig. 4. One-point correlation function (volume fractions) of the pore phase for the microstructure of the set of 2D SEM micrographs of gradient porous LSM cathode.

4. Property measurements

4.1. Electrical conductivity

Temperature dependent electrical conductivity of the half-cell LSM cathode was measured using a four-point probe method combined with a micro-heater for heating the sample up to its operating temperature (~700 °C). This method is used in order to obtain the in-plane electrical conductivity of the processed gradient porous LSM cathode and to compare the predicted in-plane values for corresponding 2D SEM images. Measurement was performed in a temperature range from 250 to 700 °C, with heating and cooling rate of 10 °C min^{-1} in the ambient atmosphere. The automechanical stage of the four-point probe setup is designed such that the tips can move up and down to make sufficient contact between the tips and the porous layer.

5. Results and discussion

The plot in Fig. 4 shows one point correlation function, i.e. variations in volume fraction of the pores (porosity %) in terms of distance from the surface of the electrode. Here, the average volume fraction of the pore phase is 0.54 which is obtained by averaging the volume fractions of the over the individual images. As shown in this plot, the volume fraction of the pores is not significantly changing through the microstructure while the corresponding SEM micrograph of the milled area reveals that the pore size is decreasing as we get close to the electrode/electrolyte interface in z direction. Fig. 5 depicts the pore-size distribution (PSD) for the microstructure of the set of 2D SEM micrographs of the gradient porous LSM cathode shown in Fig. 2. The trend shown in this plot confirms the gradient in pore size in the microstructure of the fabricated cathode as where it is desirable to have large pores to allow mass transport from the outer layers to inner layers with smaller pores at the electrode/electrolyte interface where the reaction takes place. In addition, results from the pore size distribution in these microstructures reveal that the number of pores smaller than 1 μm is increasing from surface toward the interface in the direction of porosity gradient, thus resulting in formation of more two-phase boundaries in the microstructure for electrochemical reactions. Moreover, it is clear from the distribution curves that the corresponding phase percolation is increasing in the same direction of porosity gradient.

Fig. 6 shows the two-point correlation functions (TPCF) P_2^{22} or simply P^{22} for the solid phase in the set of 2D SEM micrographs shown in Fig. 2. As we know, when r approaches to zero, the probability function gives the volume fraction of the corresponding phases. The TPCFs shown in Fig. 6 are overlapping without any significant variations in the gradient direction. Results show that all

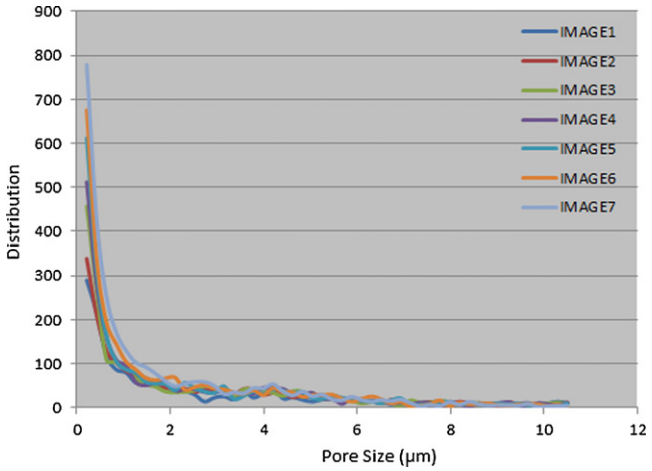

Fig. 5. Pore-size distribution functions (PSD) for the microstructure of the set of 2D SEM micrographs of gradient porous LSM cathode.

images have statistically similar two-point correlation functions, morphologies, and volume fractions, except for the size distributions. Comparison of the PSD and TPCF results also indicates that the TPCFs are regardless of the porosity gradients and thus the fabrication method (i.e. SP) is capable of generating homogeneous microstructures that are statistically identical while there is a gradient in size and distribution of one of the constituent phases. This also confirms anisotropy in z direction in terms of pore size distribution which is the main property of the developed gradient porous cathode microstructure.

The in-plane clustering of the solid phase C_2^{22} is shown based on two-point correlation cluster function (TPCCF) in Fig. 7. As shown in this plot, at higher r values, the most isolated in-plane clusters attributes to Image 1 which corresponds to the top surface layer of the cathode that are ineffective in conduction while percolation in clusters of the solid phase is gradually increasing in inner layers and is observable at the highest values in Image 5. It should be noted that the results presented here are based on 2D analysis of the in-plane microstructure of the cathode and due to columnar structure of the processed cathode, through-plane connectivity of both solid and pore phases are assumed to be preserved.

Fig. 8a–c shows percolation for the microstructure of the set of 2D SEM micrographs of the gradient porous LSM cathode in z direction from surface toward the electrode/electrolyte interface. This figure shows clusters of solid phases in different colors

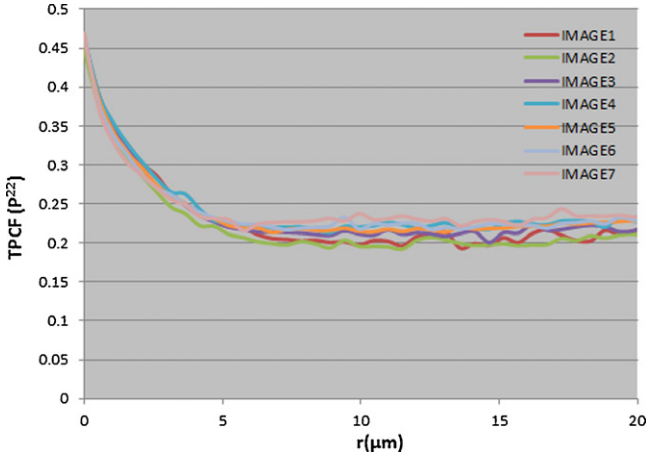

Fig. 6. Two-point correlation functions (TPCF) for the solid phase in the microstructure of the set of 2D SEM micrographs of gradient porous LSM cathode.

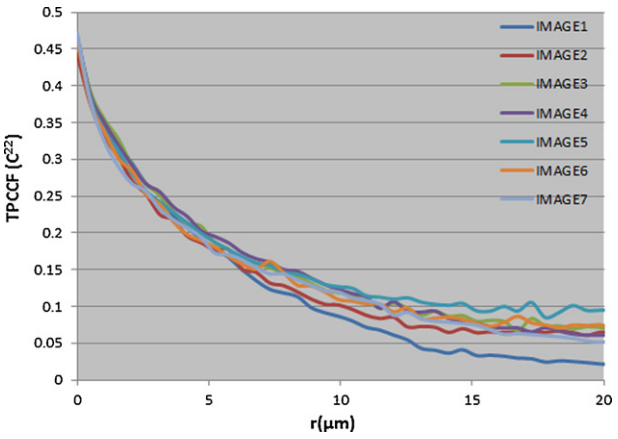

Fig. 7. Two-point correlation cluster functions (TPCCF) for the solid phase in the microstructure of the set of 2D SEM micrographs of gradient porous LSM cathode.

while the gradient in pore size as well as the particle size is clearly observable. The percolated phases are shown in the same color for graphical representation and observation of clustering of the solid phase. The solid phase (LSM) is percolated cluster in chosen microstructures in the porosity gradient direction from surface to the electrode/electrolyte interface. Connectedness of solid pore phase as the path for flowing gas is shown at each level in z direction while the in-plane pore path shrinks and distributes into smaller pores at inner layers. While percolation limit is about 30% which defines the amount of porosity required for a 3D structure to achieve cathode requirements and properties at the optimum level and also for the gas diffusion to be not rate limiting, this value is higher for a 2D structure [26,27].

While high electrical conductivity of the LSM cathode at high temperatures results in lower ohmic polarization, sufficient amount of porosity in the microstructure is required to provide a path for mass transfer through the cathode microstructure. Thus, it is important to know how the morphological changes in the microstructure affect the electrical conductivity. In order to predict the temperature dependent electrical conductivity of the gradient porous LSM cathode, electrical conductivity of the actual LSM phase with the same chemical composition of $La_{0.8}Sr_{0.2}MnO_{3+\delta}$ as the processed LSM is taken at different temperatures from the literature as the input data for the model [28]. Fig. 9 shows comparison of the predicted electrical conductivities and the experimentally measured values as a function of reciprocal temperature in air for the gradient porous LSM cathode after heat treatment in the temperature range of 200–700 °C. As shown, the electrical conductivities are increasing by increasing the temperature. The expression for the temperature dependent electrical conductivity of the small polaron materials is:

$$\sigma = \left(\frac{A}{T}\right) \exp\left(-\frac{E_a}{KT}\right) \tag{20}$$

where A is the pre-exponential factor, T is the absolute temperature, K is the Boltzmann constant, and E_a is the hopping activation energy. In general, the activation energy for electron hopping depends on the temperature and material structure. In the $La_{0.8}Sr_{0.2}MnO_3$ system, the substitution of Sr^{2+} in La^{3+} results in the formation of Mn^{4+} ions, some of which in combination with Mn^{3+} ions form Mn^{3+}–O–Mn^{4+} bonds that mostly contribute in electronic conduction. As seen in Fig. 9, the slopes of the two lines representing the activation energy for electrical conduction match in experimental and modeled data. However, the slope of the measured data is slightly increasing at 400 °C which can be attributed to the change of conduction mechanism due to change in chemical state of the material such as formation of oxygen vacancies and

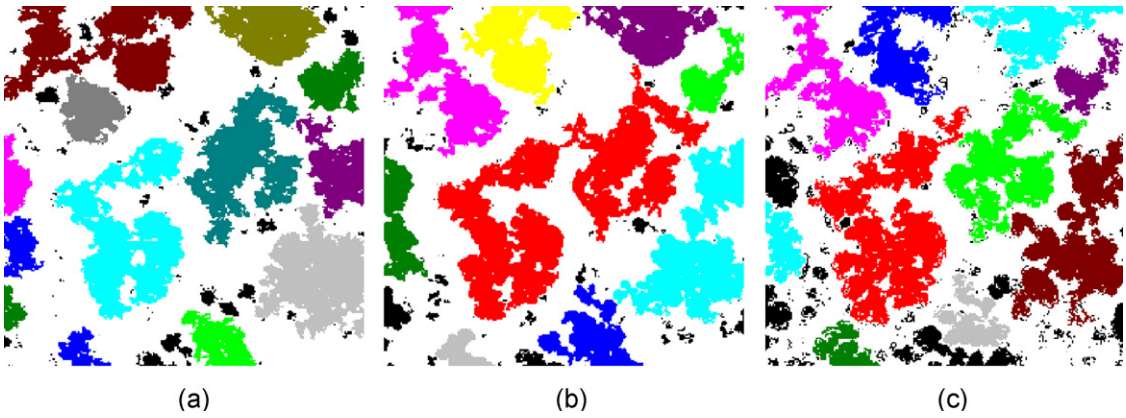

Fig. 8. Percolation for the microstructure of the set of 2D SEM micrographs of the gradient porous LSM cathode changing in the thickness direction from surface to the electrode/electrolyte interface in (a)–(c).

their contribution in ion conduction. The close values of the activation energies verify similarity in stoichiometric composition of the processed LSM material and confirm that the proposed model can only account for the effect of microstructural changes in predicted conductivity behavior [29]. Moreover, observation of a linear behavior in both plots reveals that the hopping mechanism of small polarons between $M^{3+} - M^{4+}$ pairs in this temperature range is the conduction mechanism in p-type perovskite oxide structure LSM. However, from the microstructural point of view, it is observed that the temperature dependent conductivities of the gradient porous LSM cathode are slightly lower than the predicted values; considering the amount of porosity in the processed cathode, these values are still in reasonable agreement with various experimental data reported in the literature and required for SOFC cathode application [30,31]. Due to unavailability of data on temperature dependent electrical conductivity for the exact composition of the processed sample, the input values taken from the literature may not exactly represent the actual properties of the solid phase with different morphology. Moreover, percolation is assumed to be a source of discrepancy between the experimental and theoretical data in direction of conductivity. Generally, in single-phase percolation, since the percolation limit for a 2D square lattice is higher than that in a 3D cubic one, the percolation in 3D is more readily achievable than in two dimensions. Here, due to anisotropy in the microstructure in z direction, the actual percolation limit which is strongly dependent on the distribution of the conductive phase in specific direction is different. However, due to branch-like (columnar) morphology of the processed gradient porous cathode and formation of some gaps between these columns, the in-plane 2D analysis of the gradient porous microstructure investigated in this work as well as different percolation limit of the conductive phase in the in-plane direction rather than conductance direction have resulted in overestimation of the electrical conductivity by up to an order of magnitude. Therefore, the model seems to predict a different conductivity for the gradient porous LSM than what is actually measured. In a recent work by Martinez et al., the percolation physics and a similar effect on conductivity behavior is also investigated [32].

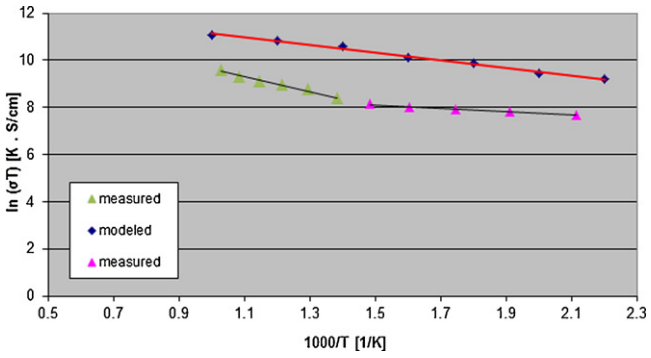

Fig. 9. Comparison between the experimental and predicted values of the temperature dependent electrical conductivity of gradient porous LSM cathode.

6. Conclusion

The statistical continuum mechanics is used to correlate properties of the gradient porous LSM cathode to its microstructure. Statistical characterization of the microstructure revealed the presence of pore size gradient in the microstructure, starting from large pores at the electrode surface and gradually decreasing the pore size toward the electrode/electrolyte interface. Results of statistical characterization also show that all images have statistically similar two-point correlation functions, morphologies, and volume fractions, except for the size distributions. Comparison of the PSD and TPCF results also indicates that the TPCFs are regardless of the porosity gradients and thus the applied fabrication method (i.e. multi-step spray pyrolysis) is capable of generating homogeneous microstructures that are statistically identical while they contain a gradient in size and distribution of one of the constituent phases. Results from TPCCF also reveal gradient in cluster size solid phase as well as the pore phase in z direction. Experimentally measured temperature dependent electrical conductivity data show slightly lower values than the predicted ones. This discrepancy can be referred to the effect of morphology and percolation effects in the porous microstructure as well as unavailability of exact conductivity data for the composition of interest. Columnar structure of highly porous gradient microstructure is also suggested as another fact responsible for the lower values of the conductivity in in-plane direction.

Acknowledgements

Authors would like to acknowledge the funding for this project from Pacific Northwest National Laboratory under Contract DE-AC05-76RL01830.

References

[1] A.S. Martinez, J. Brouwer, J. Power Sources 195 (2010) 7268.
[2] T.P. Holme, C. Lee, F.B. Prinz, Solid State Ionics 179 (2008) 1540.
[3] Y. Liu, C. Compson, M. Liu, J. Power Sources 138 (2004) 194.
[4] W. Gong, S. Gopalan, U.B. Pal, J. Electrochem. Soc. 152 (2005) A1890.
[5] G. Saheli, H. Garmestani, B.L. Adams, J. Comput. Aided Mater. Des. 11 (2004) 103.

[6] J. Deseure, L. Dessemond, Y. Bultel, E. Siebert, J. Eur. Ceram. Soc. 25 (2005) 2673.
[7] E.S. Greene, W.K.S. Chiu, M.G. Medeiros, J. Power Sources 161 (2006) 225.
[8] N.T. Hart, N.P. Brandon, M.J. Day, N. Lapeña-Rey, J. Power Sources 106 (2002) 42.
[9] S. Zha, Y. Zhang, M. Liu, Solid State Ionics 176 (2005) 25.
[10] D. Montinaro, V.M. Sglavo, M. Bertoldi, T. Zandonella, A. Arico, M.L. Faro, V. Antonucci, Solid State Ionics 177 (2006) 2093.
[11] N. Caillol, M. Pijolat, E. Siebert, Appl. Surf. Sci. 253 (2007) 4641.
[12] D. Beckel, A. Dubach, R. Studart, L.J. Gauckler, J. Electroceram. 16 (2006) 221.
[13] J. Will, A. Mitterdorfer, C. Kleinlogel, D. Perednis, L.J. Gauckler, Solid State Ionics, 131 (2000) 79.
[14] B. Ilschner, J. Mech. Phys. Solids 44 (1996) 647.
[15] H.A. Hamedani, K.-H. Dahmen, D. Li, H. Peydaye-Saheli, H. Garmestani, M. Khaleel, Mater. Sci. Eng. B 153 (2008) 1.
[16] K.O. Kjellsen, A. Monsøy, K. Isachsen, R.J. Detwiler, Cem. Concr. Res. 33 (2003) 611.
[17] M.V. Bradke, F. Gitzhofer, R. Henne, Scanning 27 (2005) 132.
[18] S. Torquato, J.D. Beasley, Y.C. Chiew, J. Chem. Phys. 88 (1988) 6540.
[19] M. Baniassadi, H. Garmestani, D.S. Li, S. Ahzi, M. Khaleel, X. Sun, Acta Mater. 59 (2011) 30.
[20] D.C. Pham, S. Torquato, J. Appl. Phys. 94 (2003) 6591.
[21] A. Mikdam, A. Makradi, S. Ahzi, H. Garmestani, D.S. Li, Y. Remond, J. Mech. Phys. Solids 57 (2009) 76.
[22] A. Mikdam, A. Makradi, S. Ahzi, H. Garmestani, D.S. Li, Y. Remond, Compos. Sci. Technol. 70 (2010) 510.
[23] S. Torquato Random Heterogeneous Materials: Microstructure and Macroscopic Properties, Springer, New York, (2002).
[24] S. Torquato, J. Appl. Phys. 58 (1985) 3790.
[25] A. Mikdam, A. Makradi, S. Ahzi, H. Garmestani, D.S. Li, Y. Remond, Int. J. Solids Struct. 46 (2009) 3782.
[26] J. Deseure, Y. Bultel, L. Dessemond, E. Siebert, P. Ozil, J. Appl. Electrochem. 37 (2007) 129.
[27] A.S. Martinez, B. Jacob, Electrochim. Acta 53 (2008) 3597.
[28] J.A.M. van Roosmalen, J.P.P. Huijsmans, L. Plomp, Solid State Ionics 66 (1993) 279.
[29] Z.C. Xia, C.Q. Tang, D.X. Zhou, J. Phys.: Condens. Matter. 13 (2001) 4359.
[30] C.-J. Li, C.-X. Li, M. Wang, Surface and Coatings Technology 198 (2005) 278.
[31] C.-C.T. Yang, W.-C.J. Wei, A. Roosen, Mater. Chem. Phys. 81 (2003) 134.
[32] N.H. Menzler, F. Tietz, S. Uhlenbruck, H.P. Buchkremer, D. Stöver, J. Mater. Sci. 45 (2010) 3109.